Jpn. J. Appl. Phys. Vol. 40 (2001) pp. 59–63
Part 1, No. 1, January 2001

Electron Paramagnetic Resonance and Photoluminescence Study of Defects in $CuGaSe_2$ Single Crystals Grown by the Traveling Heater Method

Takao NISHI*, Gennadiy A. MEDVEDKIN, Yuji KATSUMATA, Katsuaki SATO and Hideto MIYAKE[1]

Faculty of Technology, Tokyo University of Agriculture and Technology, 2-24-16 Nakacho, Koganei, Tokyo 184-8588, Japan
[1]*Faculty of Engineering, Mie University, 1515 Kamihama-cho, Tsu, Mie 514-8507, Japan*

(Received May 25, 2000; accepted for publication September 25, 2000)

Electron paramagnetic resonance (EPR) at $T = 4.2$ K and photoluminescence (PL) spectra at $T = 20$ K have been employed to elucidate point defect features in $CuGaSe_2$ crystals grown by the traveling heater method. Isotropic and anisotropic paramagnetic centers have been found in crystals as-grown and annealed in various gas mediums. Three PL bands have been observed and the influence of H_2, O_2 and Se_2 annealing has been studied. The presence of donor singlet V_{Se}^{+} has been evidenced in as-grown and H_2 annealed crystals. Complex study of EPR, PL spectra and defect physics models have allowed the addition of the point defect ensemble in $CuGaSe_2$ with defect pairs $(2V_{Cu}^{-}+Ga_{Cu}^{2+})$, V_{Cu} and other defect complexes, according to treatments used in this work.

KEYWORDS: $CuGaSe_2$ crystals, electron paramagnetic resonance (EPR), photoluminescence (PL), selenium vacancy (V_{Se}^{+}), complex defects

1. Introduction

$CuGaSe_2$ is a promising absorber material for photovoltaic devices because of its appropriate band gap and high absorption coefficient in the solar spectrum. In spite of considerable progress in research relating to its solar-cell application, limited data are available regarding the basic properties of this material. To improve the material quality, a greater knowledge of the electronic structure must be obtained via systematic studies of point defects and impurities in single crystals. Only a few studies have been carried out on Cu-vacancies (V_{Cu}) and Fe- and Ni-related centers in $Cu(In,Ga)Se_2$ semiconductors using the electron paramagnetic resonance (EPR) technique.[1–5] The only available EPR data for polycrystalline $CuGaSe_2$ prepared by the melt growth method were reported by Birkholz *et al.*[2] Recently, the traveling heater method (THM) was employed for the growth of $CuGaSe_2$ single crystals with a low concentration of impurities.[6] However, unintentional donors and acceptors of a measurable concentration exist in all $CuGaSe_2$ crystals and considerable efforts are being put forth by many research groups towards defect control and characterization. It was found previously that the post-growth annealing of Cu-containing ternary selenides in air or oxygen improves the optical properties of single-crystal thin films[7] and increases the efficiency of polycrystalline solar cells.[8,9] The mechanism responsible for this oxygen annealing effect has not been fully understood or explained until now. Annealings, like growth conditions, strongly affect the intrinsic defect ensemble and unintentional impurities in $CuGaSe_2$, significantly modifying its optical and electrical properties. The objective of this study is to provide new information on point defects using low-temperature measurements of EPR and photoluminescence (PL) spectra and to elucidate the annealing effect on $CuGaSe_2$ single crystals.

2. Experimental

Bulk $CuGaSe_2$ crystals were grown from a Ga solution using the THM at Mie University.[6] Measured samples were cut out of the bulk material and have typical sizes of $4 \times 2 \times 2\,mm^3$. In order to control the extrinsic/intrinsic defect concentration the samples were subjected to annealing in Se_2, O_2, and H_2 atmospheres. Se_2 annealing was carried out in a closed processing tube. The sample was sealed in an evacuated quartz ampoule of 0.8 cm diameter and 20 cm length that also contained the Se powder placed at the other end of this ampoule. O_2 and H_2 treatments were carried out in an open processing tube. The sample was placed in a quartz tube of 20 cm diameter and 100 cm length. The tube was filled with annealing gas of about 2 atm in pressure. The above-mentioned annealings were carried out at 200°C for 1 h. A JEOL JES-RE2X X-band spectrometer was employed in the EPR measurements. A magnetic field up to 1.3 T and a microwave power of 5 mW was used. The samples mounted in a cryostat at 4.2 K were oriented in various directions relative to the magnetic field and crystallographic axes. PL measurements were performed using an Ar^+ laser (514.5 nm, 30 mW), a JASCO CT-25C monochromator and a North Coast EO-817L model Ge photodiode cooled with liquid nitrogen. A sample temperature of 20 K was maintained using a cryomini-type He-refrigerator cryostat.

3. Results and Discussion

3.1 Electrical conductivity

The thermal probe method reveals that the p-type conductivity remains for all the samples before and after treatments. The magnitude of thermo-e.m.f. varies but the conductivity type was the same, regardless of the gaseous surrounding (Se_2, H_2, O_2). Thus, no undertaken annealing gives rise to n-type conductivity. This feature of $CuGaSe_2$ is in accordance with the phenomenological doping pinning rule.[10,11] The estimation of specific conductivity by the VA-ohm meter gives values of $\sigma \leq 2 \times 10^{-7}\,\Omega^{-1}cm^{-1}$ for as-grown and H_2 annealed samples, and $\sigma \leq 2 \times 10^{-5}\,\Omega^{-1}cm^{-1}$ for Se_2 and O_2 annealed samples at $T = 300$ K. The steady p-type conductivity and high resistivity indicate a high power of donor-acceptor (D-A) compensation in $CuGaSe_2$ crystals. The increase of the σ value by two orders as a result of Se_2 or O_2 annealing indicates the change in free hole concentration, most likely caused by the donor V_{Se} point defects. As known from previous investigations,[12–14] selenium and oxy-

*E-mail address: takawou@cc.tuat.ac.jp

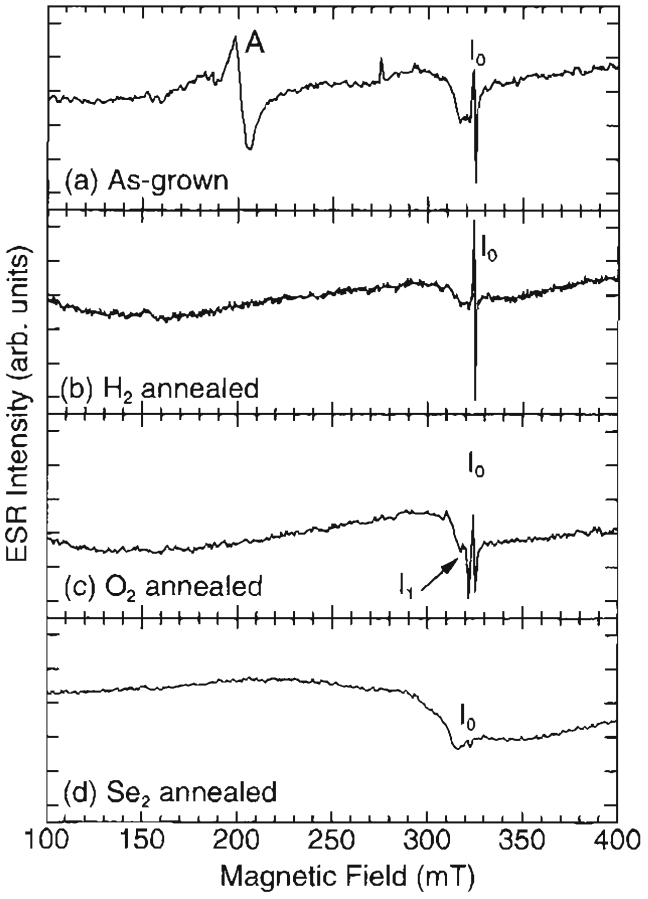

Fig. 1. EPR spectra of $CuGaSe_2$ single crystals at $T = 4.2$ K and $\nu = 9.1$ GHz: (a) as-grown, (b) H_2 (c) O_2 and (d) Se_2 annealed samples.

gen usually serve as efficient chemical agents in Cu-III-Se_2 materials to suppress surplus donor-type point defects such as V_{Se}; therefore, our treatments should result in a decrease of D-A compensation.

3.2 *Annealing effect on EPR spectra*

The EPR spectra of samples as-grown and annealed in H_2, O_2, and Se_2 atmospheres are presented in Fig. 1. All of the curves show the peak signal I_0 at the magnetic field $H = 320$ mT. An additional EPR peak was detected in the low magnetic field region, denoted A. There are no other signals in the range $H = 0$–1.3 T.

The g-factor was elucidated for I_0 signal as 2.006, close to $g = 2.0023$ for free electrons. The narrow line ($\Delta H_{pp} \approx 0.8$ mT) is characteristic of all EPR spectra excluding the Se_2 treated crystal. This difference is associated with the concentration of selenium atoms or selenium vacancies in the crystals. Since the decrease of the EPR I_0 signal is observed only after annealing with group VI elements (*e.g.*, oxygen, selenium), this effect may be ascribed to decreasing the V_{Se} concentration. Previously, EPR signals were observed at around $g = 2.003$ in Cu(In,Ga)Se_2 and $CuIn_2Se_{3.5}$ compounds[2–4] and tentatively assigned to singly ionized donors as anticipated V_{Se}^+ and Ga_{Cu}^+. For binary chalcogenides, the EPR signals at $g = 2.0027$ with the linewidth of 0.58 mT in ZnSe epilayers, ZnS ($g = 2.0034$), CaSe (2.003) and SrSe (2.0032) were also assigned to the singly ionized anion vacancy[15,16] hyperfine structure (HFS) in our EPR spectra due to hyperfine interaction with the nuclear spins of Cu, Ga, and Se. Copper has the isotope ^{63}Cu (abundance of 69.2%), ^{65}Cu (30.8%), and both have the nuclear spin $I = 3/2$. The spin of ^{69}Ga and ^{71}Ga is $I = 3/2$, and the abundance is 60.2% and 39.8%, respectively. The nuclear spin of ^{77}Se (7.6%) is $I = 1/2$. Therefore, the electron spins on the point defects as V_{Se}^+ in $CuGaSe_2$ single crystal are influenced from these nuclear spins, essentially, and a HFS should be observed in EPR signals. However, clear hyperfine splitting was not observed in our experiments with THM-grown $CuGaSe_2$ crystals (see Fig. 1). The result may be associated with the overlapping of a large number of nuclear spins, or the influence of the defect concentration. Previously, the HFS responsible for the isotope ^{67}Zn (nuclear spin $I = 5/2$) was observed in the EPR signal of the V_S vacancy in ZnS.[15] The high donor concentration ($\sim 10^{18}$ cm^{-3}) usually results in a single narrow line in EPR spectra due to exchange coupling between close pairs of donor defects. Since this effect was also found in $CuInSe_2$,[3] we expect that our crystals of $CuGaSe_2$ have a high concentration of V_{Se}, estimated roughly as $>10^{18}$ cm^{-3}. As known from the defect physics of ternary compounds discussed in refs. 17 and 18, the formation energies for various point defects in chalcopyrites differ significantly and for $CuGaSe_2$ by analogy they may be ranged as

$$Ga_{Cu} < Cu_{Ga} < V_{Se} < V_{Cu} < V_{Ga} < Cu_i. \quad (1)$$

Our crystals were grown by the THM using Ga solution; thus the presence of point defects such as Cu_{Ga}, V_{Ga} and Cu_i is unlikely. On the other hand, the formation of some point defect complexes occurs with a lower formation energy than single point defects, *e.g.*, $(2V_{Cu}^- + In_{Cu}^{2+})$ and $(Cu_{In}^{2-} + In_{Cu}^{2+})$ in $CuInSe_2$.[18,19] Based on defect physics models we assume that the main point defects in our $CuGaSe_2$ crystals are V_{Se} (V_{Se}^0, V_{Se}^+ or V_{Se}^{2+}), a $(2V_{Cu}^- + Ga_{Cu}^{2+})$ defect pair and V_{Cu}^-. Clearly, the charge state may change with treatments. Because the neutral and doubly ionized centers are not paramagnetic, the EPR measurements reveal the presence of singly ionized defects such as V_{Se}^+ and $(V_{Cu}^- + Ga_{Cu}^{2+})^+$ or V_{Cu}^-. It should be noted that, energetically, the existence of the first two defects is preponderant in our crystals. Thus, Se_2 and O_2 annealings lead to the suppression of selenium vacancies, gallium antisite defects and reduce the EPR signal (see Fig. 1). The corresponding chemical reactions are expressed:

Se_2 annealing

$$V_{Se}^{2+} + \frac{1}{2}Se_2 \rightarrow Se_{Se}^0. \quad (2)$$

O_2 annealing

$$\text{Major:} \quad 2(2V_{Cu}^- + Ga_{Cu}^{2+})^0 + \frac{3}{2}O_2 \rightarrow 4V_{Cu}^- + Ga_2O_3,$$

$$\text{Major:} \quad (2V_{Cu}^- + Ga_{Cu}^{2+})^0 + \frac{1}{2}O_2 \rightarrow 2V_{Cu}^- + GaO,$$

$$\text{Minor:} \quad V_{Se}^{2+} + \frac{1}{2}O_2 \rightarrow (V_{Se}^{2+} + O^{2-})^0. \quad (3)$$

In the case of Se_2 annealing, the more effective suppression of V_{Se} occur; however, in the case of O_2 annealing, the additional formation of more complex defects such as oxide molecules is possible. The similar production of oxide

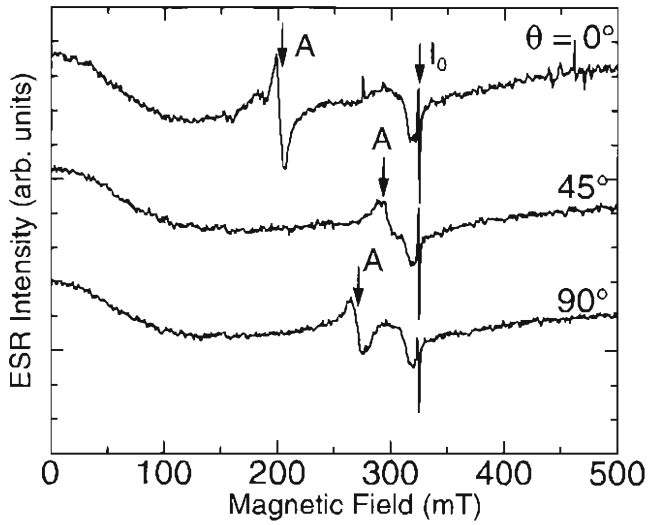

Fig. 2. Anisotropy of EPR in $CuGaSe_2$ single crystals. Various orientations of the tetragonal axis c and the magnetic field $\boldsymbol{H}$ are marked along with the EPR curves ($\theta = 0°$ corresponds to $c \| \boldsymbol{H}$).

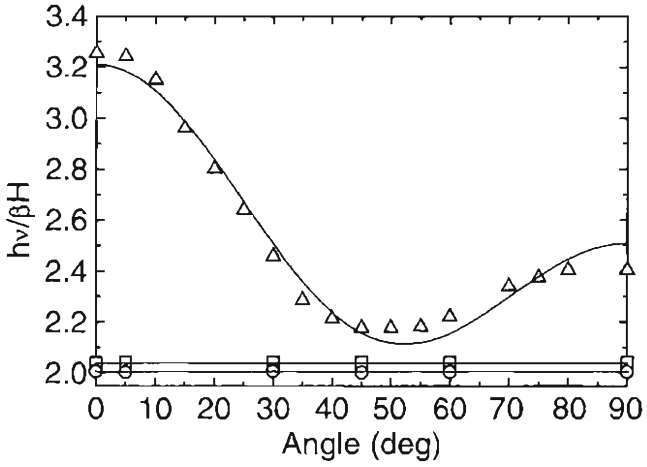

Fig. 3. Angular dependence of EPR signals. Points experiment: A (△) anisotropic, I_0 (○) and I_1 (□) isotropic signal for as-grown and annealed samples. Solid line: calculation from eq. (5).

interaction with the chalcopyrite lattice in the first stage of thermal oxidation and ion implantation.[13,14]

As seen in Fig. 1(c), the I_1 peak signal appears ($g_{\text{average}} = 2.04$, $\Delta H_{\text{pp}} \approx 2\,\text{mT}$). The additional I_1 peak that arose may be responsible for the electrically polarized Ga-O bonds (non-neutral). This structure appears due to the changing coordination of Ga atoms in the chalcopyrite lattice because of reacting oxygen and the formation of new molecular complexes Ga_2O_3, GaO, $(GaO)^+$ with V_{Cu}^-. In contrast to the treatments discussed above, the H_2 annealing should have the opposite effect on the point defect ensemble. The high concentration of acceptor-type defects V_{Cu} in the initial crystals should be partly suppressed by intensive H_2 annealing. It is assumed that the hydrogen in $CuGaSe_2$ passivates the main defects responsible for p-type conductivity. Although the type of conductivity cannot be changed in the opposite p → n direction as in the oxygen interaction,[13,14] the passivation of the surface and improvement of crystal quality are expected. In our experiments, the most probable chemical reaction is flowing to:

H_2 annealing

$$(2V_{Cu}^- + Ga_{Cu}^{2+})^0 + \frac{1}{2}H_2 \rightarrow (V_{Cu}^- + Ga_{Cu}^{2+})^+ + (V_{Cu}^- + H^+)^0. \quad (4)$$

In other words, the H_2 annealing results in the increasing concentration of singly charged point defect pairs $(V_{Cu}^- + Ga_{Cu}^{2+})^+$ due to the H_2 passivation of copper vacancies. Indeed, the EPR I_0 signal in hydrogen treated crystals has the maximum amplitude [see Fig. 1(b)]. This indicates the elevated concentration of singlet paramagnetic centers after the H_2 annealing.

3.3 *Anisotropic EPR*

Apart from the I signals in EPR spectra, we have found the low-field A signal that possesses the properties of an anisotropic line. Figure 2 shows three EPR spectra for the as-grown $CuGaSe_2$ single crystal at various orientations of the tetragonal axis c and magnetic field $\boldsymbol{H}$. As is evident, the wide swing of the anisotropic shift is brought about by changing the angle θ. Annealings in the Se_2, O_2 or H_2 environment result in the disappearing A signal. This anisotropic center shows angular dependence on the θ angle (see Fig. 3), and reveals the maximal coefficient of anisotropy of $(g_{\text{eff}\|} - g_{\text{eff}\perp})/(g_{\text{eff}\|} + g_{\text{eff}\perp}) \times 100\% = 20\%$. The nature of this anisotropic center is not clear at present. One can consider two possibilities. First, we can assume that the A signal may be associated with some transitional metals with a d^7 electron configuration (Fe^+, Co^{2+} or Ni^{3+}) that were measured in II–VI compounds[20,21] and showed a similar angular dependence of A signals. Second, we can assume that the excess gallium in the starting crystals allows the existence of Ga defects as interstitials or Frenkel pairs. Both treatment by H_2, O_2, Se_2 annealing, and the test annealing in vacuum carried out at low temperature $T = 200°C$ give rise to the disappearance of the EPR anisotropic signal. Thus, we can assume that there is a the low-energy annihilation of the Frenkel Ga defect pairs and ordering in the Ga cation sublattice of $CuGaSe_2$ for 1 h heating. To fit our experimental data, we used spin Hamiltonian approach for a $3d^7$ ion with tetrahedral cubic symmetry by the following expression

$$g_{\text{eff}}(\theta) = \frac{h\nu}{\beta H} = g - \frac{9u}{5}\left(1 - \frac{5}{4}\sin^2\theta(1 + 3\cos^2\theta)\right), \quad (5)$$

where $h\nu$ is the microwave energy, β the Bohr magneton, H the applied magnetic field, and u the fitting coeffcient. The first term in eq. (5) gives the conventional Zeeman interaction, and the second term is one that has been presented by Bleaney[22] and Koster and Statz[23] and is allowed by the symmetry. Figure 3 shows the fitting curve which well describes the experimental data. The A signal anisotropy is found to be 10^2–10^3 times larger than that for II–VI cubic compounds in the same magnetic field. Similar strong anisotropic signals were also reported for other chalcopyrite semiconductors such as $CuAlS_2$, $CuGaS_2$, and $AgGaS_2$.[24] The EPR anisotropy observed in our $CuGaSe_2$ crystals may be associated with a defect center of a lowered local symmetry assigned by the tetragonal field of the chalcopyrite lattice and distorted by nearest ion neighbours. Details of the anisotropic

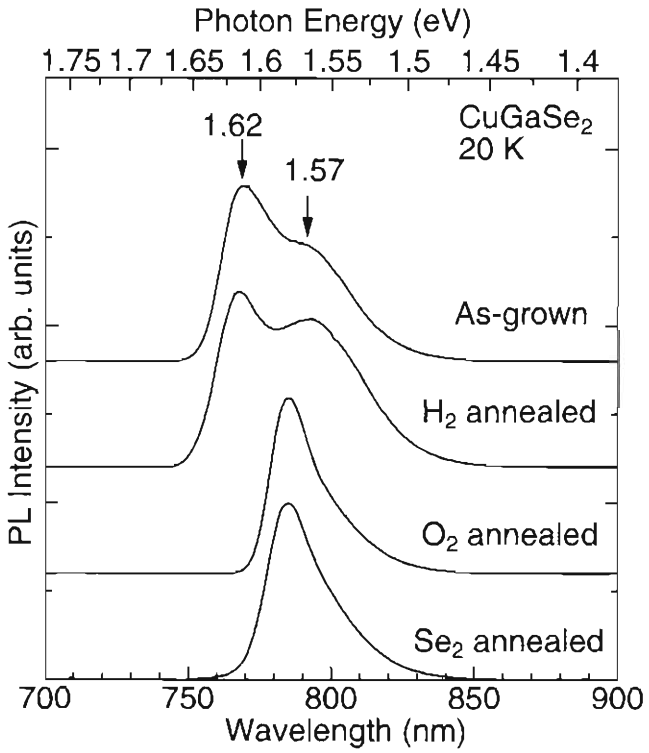

Fig. 4. Photoluminescence spectra at $T = 20$ K of $CuGaSe_2$ single crystals as-grown and annealed in various mediums.

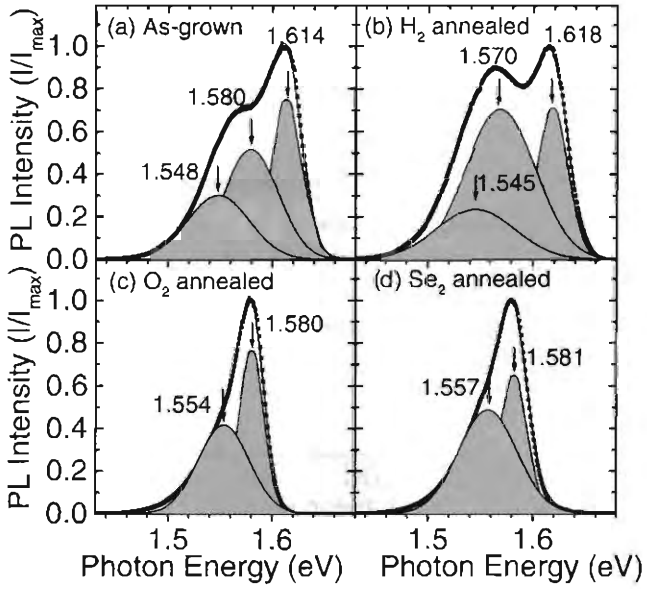

Fig. 5. Multipeak Gaussian fit to photoluminescence spectra of $CuGaSe_2$ single crystals as-grown (a) and annealed in various mediums (b)–(d). The common fitting curve well traces the experimental points. Shadowed contours: uniformly broadened lines.

EPR study will be reported in a later publication. Unlike the A center, the I centers have no paramagnetic anisotropy. The isotropic feature of the I signals in the EPR spectra remains after all the treatments. It is known that the signal due to defects with a shallow level or of a high concentration usually exhibits isotropy. Wave functions of an electron on the shallow defect essentially have an s-character. From PL measurements (see §3.4 and refs. 25 and 26) it is evident that the donor level of the V_{Se} defect lies 80–100 meV below the conduction band and thus it cannot be correctly described in terms of a hydrogen-like model. Therefore, the main reason for the isotropy of the I signals are the elevated concentration ($>10^{18}$ cm^{-3}) of these defects in the THM-grown $CuGaSe_2$ single crystals.

3.4 Photoluminescence

The treatments used do not significantly change the integral PL response; the entire intensity varied, at the most, two times. The PL spectra of all the samples under study are presented in Fig. 4. Two emission bands are observed at 1.57 and 1.62 eV for both as-grown crystals and H_2 annealed ones. Similar PL emissions were reported for $CuGaSe_2$ epitaxial films grown by molecular beam epitaxy[7,25] and are close to those reported in ref. 27 for $CuGaSe_2$ single crystals grown by iodine vapor transport. Taking into account the different laser pumping energies and temperatures of PL measurements and using the temperature coefficient $dE_g/dT = -2.1 \times 10^{-9}$ eV/K for $CuGaSe_2$ as an estimation, one may declare a good agreement of our PL measurements with that at $T = 2$ K[7,25] and some divergence with that at 110 K.[27] The main PL emission peaks at $h\nu = 1.614$–1.618 eV in as-grown and H_2 annealed samples. Annealing in different mediums (i.e., Se_2 and O_2) leads to the disappearance of this band and the 1.57–1.58 eV band prevails over others. On the other hand, the EPR spectra in Figs. 1(c) and 1(d) show that annealing in selenium suppresses the I_0 peak more effectively than annealing in oxygen. This implies that the O_2 annealing compensates V_{Se} vacancies only partly and simultaneously generates other oxygen related defect complexes, as mentioned in §3.2. As follows from our EPR results and the PL data of other studies,[7,25,27] the short wavelength peak (1.62 eV) may be ascribed to the V_{Se}^{+} point defect in as-grown and H_2 annealed crystals. The existence of selenium vacancies in other charge states is also plausible but their existence requires confirmation. Thus, after Se_2 or O_2 treatments, the concentration of V_{Se} falls rapidly with the formation of neutral Se_{Se} or $(V_{Se}^{2+} + O^{2-})$ states, accordingly. However, the double I_0–I_1 peak in the EPR spectra [Fig. 1(c)] unambiguously indicates the existence of charged defect complexes with oxygen such as Ga_2O_3, GaO, $(GaO)^+$ with V_{Cu}^{-} or $(V_{Se}^{-} + O^{2-})^{-}$. The H_2 annealing had an opposite effect on the $(2V_{Cu}^{-} + Ga_{Cu}^{2+})$ state, slightly activating the Ga_{Cu} point defect by the charged defect pair $(V_{Cu}^{-} + Ga_{Cu}^{2+})^{+}$. In terms of the hydrogen effect on the crystal, it is believed that the change in the V_{Se} concentration is minimal.

Figure 5 presents the spectral analysis of PL spectra measured for as-grown, H_2, O_2 and Se_2 annealed samples. The fitting parameters are summarized in Table I. Here we used a multipeak Gaussian fit and obtained a good tracing of the fitting curves over all of the experimental points. As follows from Figs. 5(a) and 5(b), the common spectral contour can be resolved into three single uniformly broadened lines at 1.614–1.618 eV, 1.570–1.580 eV and 1.545–1.548 eV. As follows from Figs. 5(c) and 5(d), only two single uniformly broadened lines can be extracted from the experimental data for O_2 and Se_2 annealed samples. The observed lines peak at 1.580–1.581 eV and 1.554–1.557 eV. Additionally, the spectral analysis allows to retrieve an uncertain PL band at long wavelengths. The wide spectral band (full-width at half maximum (FWHM) = 60–90 meV) at around 1.55 eV was found

Table I. Fitting parameters for PL spectra of $CuGaSe_2$ single crystals.

Treatment	Line no.	Peak (eV)	FWHM (meV)	Height
As-grown	1	1.614	33.7	0.759
	2	1.580	61.7	0.517
	3	1.548	69.8	0.301
H_2 annealed	1	1.618	34.4	0.713
	2	1.569	77.6	0.705
	3	1.545	87.5	0.235
O_2 annealed	1	1.580	27.8	0.778
	2	1.554	57.8	0.417
Se_2 annealed	1	1.581	31.0	0.661
	2	1.557	65.3	0.483

to retain in all PL spectra, see Table I and Figs. 5(a) to 5(d). These two long wavelength emissions may be ascribed to optical transitions between some point defect states that are not affected by treatments used in this work. They may be a steady defect complex in $CuGaSe_2$ with a very low formation energy, for example $(Cu_{Ga}^{2-} + Ga_{Cu}^{2+})$, similar to theoretical predictions[18,19] for $CuGaSe_2$ and $CuInSe_2$. Further study is required to elucidate the nature of these long wavelength PL bands in $CuGaSe_2$ single crystals through implication of the defect center concentration, their charge state and their energy position in the forbidden gap of the semiconductor.

4. Conclusions

This paper describes new EPR and PL features of the point defect ensemble in $CuGaSe_2$ single crystals grown by the THM. The EPR spectra exhibit variation in the strength of the isotropic I lines for as-grown crystal and others subjected to annealing in H_2, O_2 and Se_2 mediums. The additional anisotropic EPR-signal (A line) has been found in the as-grown $CuGaSe_2$ crystals only and its angular dependence was measured. The EPR spectra allowed us to define the paramagnetic properties and a g-factor of 2.006 for the point defect centers in $CuGaSe_2$ and to link them with the presence of singly ionized defects V_{Se}^{+}, V_{Cu}^{-} and a defect pair $(V_{Cu}^{-} + Ga_{Cu}^{2+})^{+}$. The formation of Ga-O bonds and oxygen-related complexes as a result of O_2 annealing has been revealed by the additional EPR I_1 line. The photoluminescent properties of these $CuGaSe_2$ single crystals were examined and three emission bands have been found. The 1.62 eV band was ascribed to optical transitions from the V_{Se}^{+} donor level. The long wavelength emissions have been found to not be affected by various treatments and may be associated with some stable defect pairs such as $(Cu_{Ga}^{2-} + Ga_{Cu}^{2+})$.

Acknowledgements

The authors are grateful to the Japanese Society for the Promotion of Science for their support of this research.

1) R. Rai, S. K. Gupta, D. K. Suri and S. Z. Ali: Phys. Status Solidi B **124** (1984) K167.
2) M. Birkholz, P. Kanschat, T. Weiss, M. Czerwensky and K. Lips: Phys. Rev. B **59** (1999) 12268.
3) K. Sato, N. Nishikawa, I. Aksenov, T. Shinzato and H. Nakanishi: Jpn. J. Appl. Phys. **35** (1996) 2061.
4) J. M. Tchapkui-Niat, A. Goltzene and C. Schwab: J. Phys. C **15** (1982) 4671.
5) H. J. von Bardeleben and R. D. Tomlinson: J. Phys. C **13** (1980) L1097.
6) H. Miyake: Recent Dev. Bulk Cryst. Growth **9** (1998) 271.
7) S. Niki, P. J. Fons, A. Yamada, R. Suzuki, T. Ohdaira, S. Ishibashi and H. Oyanagi: *Proc. 11th Int. Conf. Ternary and Multinary Compounds, Salford, U.K., September 1997*, Inst. Phys. Conf. Ser. **152** (1998) 221.
8) R. Noufi, R. C. Powell and R. J. Matson: Sol. Cells **21** (1987) 55.
9) R. E. Hollingsworth and J. R. Sites: Sol. Cells **16** (1986) 457.
10) S. B. Zhang, S. H. Wei and A. Zunger: J. Appl. Phys. **83** (1998) 3192.
11) W. Walukiewicz: J. Vac. Sci. & Technol. **B5** (1987) 1062.
12) G. A. Medvedkin and M. A. Magomedov: J. Appl. Phys. **82** (1997) 4013.
13) G. A. Medvedkin, M. V. Yakushev, A. E. Hill, R. D. Pilkington and R. D. Tomlinson: Cryst. Res. Technol. **31** (1996) 209.
14) M. E. Boiko and G. A. Medvedkin: Sol. Energy Mater. & Sol. Cells **41/42** (1996) 307.
15) S. D. Setzler, M. Moldovan, Z. Yu, T. H. Myers, N. C. Giles and L. E. Halliburton: Appl. Phys. Lett. **70** (1997) 2274.
16) J. E. Wertz, J. W. Orton and P. Auzins: Discuss. Faraday Soc. **31** (1961) 140.
17) H. Neumann: Cryst. Res. Technol. **18** (1983) 901.
18) S. B. Zhang, S. H. Wei and A. Zunger: Phys. Rev. B **57** (1998) 9642.
19) A. Zunger, S. B. Zhang and S. H. Wei: Proc. 26th IEEE PV Spec. Conf., Anaheim CA, USA, 1997, p. 313.
20) W. C. Holton, J. Schneider and T. L. Estle: Phys. Rev. **133** (1964) A1638.
21) F. S. Ham, G. W. Ludwig, G. D. Watkins and H. H. Woodbury: Phys. Rev. Lett. **5** (1960) 468.
22) B. Bleaney: Proc. R. Soc. A **73** (1959) 939.
23) G. F. Koster and H. Statz: Phys. Rev. **113** (1959) 445.
24) U. Kaufmann, A. Rauber and J. Schneider: Solid State Commun. **15** (1974) 1881.
25) A. Yamada, P. Fons, S. Niki, H. Shibata, A. Obara, Y. Makita and H. Oyanagi: J. Appl. Phys. **81** (1997) 2794.
26) J. H. Schon and E. Bucher: Sol. Energy Mater. & Sol. Cell **57** (1999) 229.
27) M. Susaki, T. Miyauchi, H. Horinaka and N. Yamamoto: Jpn. J. Appl. Phys. **17** (1978) 1555.